RSC Advances

PAPER

View Article Online
View Journal | View Issue

Cite this: *RSC Adv.*, 2021, **11**, 11976

Triazine bis(pyridinium) hydrogen sulfate ionic liquid immobillized on functionalized halloysite nanotubes as an efficient catalyst for one-pot synthesis of naphthopyranopyrimidines†

Marzieh Samadani, Beheshteh Asadi, Iraj Mohammadpoor-Baltork,* Valiollah Mirkhani, Shahram Tangestaninejad and Majid Moghadam

Received 15th February 2021
Accepted 15th March 2021

DOI: 10.1039/d1ra01230d

rsc.li/rsc-advances

1,1′-(6-(Propyl amino)-1,3,5-triazine-2,4-diyl)bis(pyridinium) hydrogen sulfate immobillized on halloysite nanotubes [(PATDBP)$(HSO_4)_2$@HNT] as a solid acid nanocatalyst was successfully synthesized and characterized by various analysis techniques such as FT-IR, TGA, SEM/EDX, elemental mapping, TEM and elemental analysis. This catalyst was found to be highly efficient for the convenient synthesis of naphthopyranopyrimidine derivatives through a one-pot three-component reaction of β-naphthol, aldehydes and *N*,*N*-dimethylbarbituric acid in excellent yields under solvent-free conditions. Furthermore, the catalyst could be recovered and reused five times without any notable loss of its activity.

Introduction

Ionic liquids (ILs) have become quite famous in recent years owing to the unique properties of extremely low vapor pressure, tunable polarity, nonflammability, large liquid range, high stability, and wide solubility.[1] However, the widespread application of ILs as homogeneous catalysts and solvents has been limited by drawbacks such as difficulties in separating from the reaction mixture and recycling as well as high cost. To overcome these issues, supported ionic liquids have been introduced and used as heterogeneous and recoverable catalysts.[2] Among different supports, halloysite nanotubes (HNTs) with a molecular formula of $Al_2Si_2O_5(OH)_4 \cdot 2H_2O$ (1 : 1 ratio of Al/Si) have gained special attention due to the advantages such as environmental friendliness, high mechanical and thermal stability, biocompatibility, low price, large surface area, ease of reusability, and resistibility against organic solvents.[3] As a result, using HNTs as supports is greatly attractive in the fields of catalysis in organic transformations,[4] industry[5] as well as pharmaceutical studies.[6]

Multicomponent reactions[7] (MCRs) are convergent procedures in which three or more precursor components are jointed in a single operation to afford the final product. These reactions offer many advantages over stepwise reaction, such as less waste generation and high atom economy. Moreover, molecular diversity with minimal synthetic effort is created using different reactants. One of the most important applications of MCRs is found in heterocycle chemistry.[8] Combination of both N- and O-heterocyclic scaffolds are a group of promising molecular frameworks with many notable biological and pharmacological properties. Accordingly, research on the synthesis of naphthopyranopyrimidines[9] with potent antimicrobial,[10] anticonvulsant,[11] antibacterial[12] and antifungal[13] activities, has been developed. Consequently, the growth of new sustainable catalytic system for the synthesis of fine chemicals is still of great significance. In this sense and also, in continuation of our previous works,[14] we herein report the synthesis and application of 1,1′-(6-(propyl amino)-1,3,5-triazine-2,4-diyl)bis(pyridinium) hydrogen sulfate immobillized on functionalized halloysite nanotubes [(PATDBP)$(HSO_4)_2$@HNT] as a recoverable and reusable catalyst for the synthesis of naphthopyranopyrimidine derivatives *via* a three-component reaction under solvent-free conditions (Scheme 1).

Results and discussion

Preparation and characterization of heterogeneous 1,1′-(6-(propyl amino)-1,3,5-triazine-2,4-diyl)bis(pyridinium) hydrogen sulfate ionic liquid [(PATDBP)$(HSO_4)_2$@HNT]

The synthesis of the nanocatalyst [(PATDBP)$(HSO_4)_2$@HNT] follows the stages depicted in Scheme 2. First, HNT was reacted with 3-aminopropyltriethoxysilane (APTS) under microwave irradiation to furnish suitable surface because of major functionalization affording PA@HNT. Covalently, 1,3,5-trichlorotriazine (TCT) was immobilized onto the surface of the nano-clay through formation of C–N bond by controlling the temperature[7e] to provide PAT@HNT and followed by addition of

Department of Chemistry, Catalysis Division, University of Isfahan, Isfahan 81746-73441, Iran. E-mail: imbaltork@sci.ui.ac.ir; Tel: +98 31 3793 4927

† Electronic supplementary information (ESI) available. See DOI: 10.1039/d1ra01230d

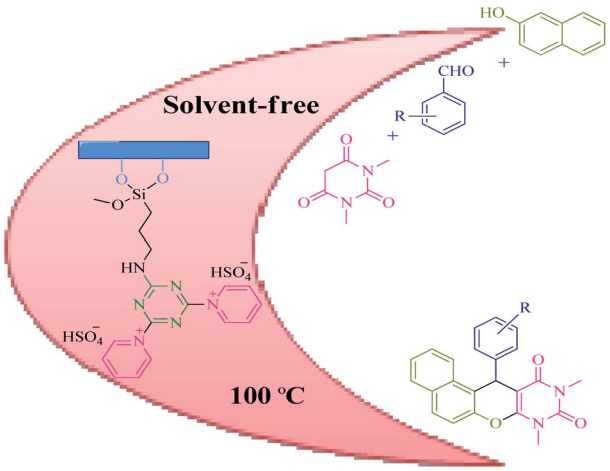

Scheme 1 Synthesis of naphthopyranopyrimidines catalyzed by [(PATDBP)$(HSO_4)_2$@HNT].

pyridine and *N*,*N*-diisopropylethylamine (DIPEA) to give nano-clay modified with 1,1′-(6-(propyl amino)-1,3,5-triazine-2,4-diyl)bis(pyridinium) chloride IL. Finally, [(PATDBP)$(HSO_4)_2$@-HNT] was prepared by the reaction of [(PATDBP)Cl_2@HNT] with $NaHSO_4$ in Mili-Q water (Scheme 2).

These steps were probed by FT-IR, thermogravimetric analysis (TGA), SEM/EDX, elemental mapping, TEM and elemental analysis (EA).

The FT-IR spectrum of halloysite nanotubes displays several characteristic peaks at 3695 and 3625 cm^{-1}, 910 cm^{-1}, 1034 and 468–535 cm^{-1}, attributing to the OH groups, bending vibration of Al–OH, Si–O stretching and Si–O bending vibrations, respectively (Fig. 1a).[15] New peaks appear after modification by APTS, at 3352–3446 cm^{-1} (NH_2 stretching vibration), 2874–2930 cm^{-1} (C–H stretching vibration) and 1585–1640 cm^{-1} (NH_2 bending vibration) indicating successful attachment of linker to the surface of nano-clay (Fig. 2b). As shown in Fig. 1c, the FT-IR spectrum of PAT@HNT show characteristic peaks at

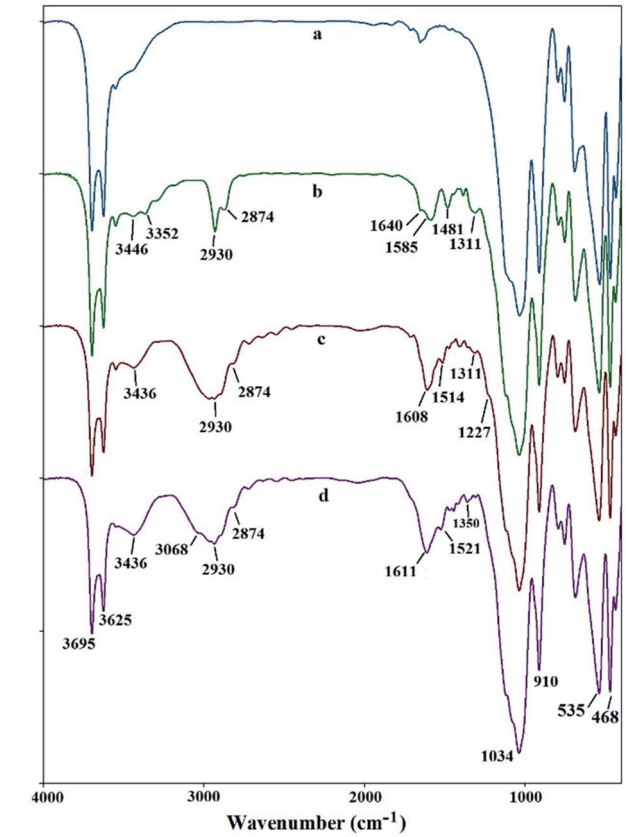

Fig. 1 Comparison of the FT-IR spectra of (a) HNTs; (b) PA@HNT; (c) PAT@HNT; (d) [(PATDBP)Cl_2@HNT].

around 3436 (NH stretching vibration), broad peak at 1608 (C=N), 1514 (NH bending vibration) and at 1227–1311 cm^{-1} (C–N stretching vibration). It should be noted that, the C–Cl band of TCT at 1035–1100 cm^{-1} was masked owing to the presence of strong Si–O stretching band at 1000–1100 cm^{-1}. Also, the absorption band at 3068 and broad peak at 1611 cm^{-1} in Fig. 1d may confirm that the pyridine ring is truly attached.

The TGA curve of the catalyst is shown in Fig. 2. A slower mass loss was observed in the first-stage with a weight loss of 4.59% (30–180 °C) which corresponds to the water evaporation. The major weight loss was observed between 180 to 580 °C in

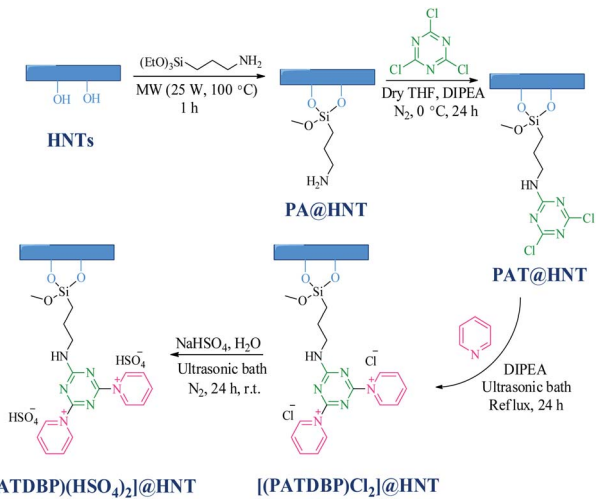

Scheme 2 Synthesis of nanocatalyst [(PATDBP)$(HSO_4)_2$@HNT].

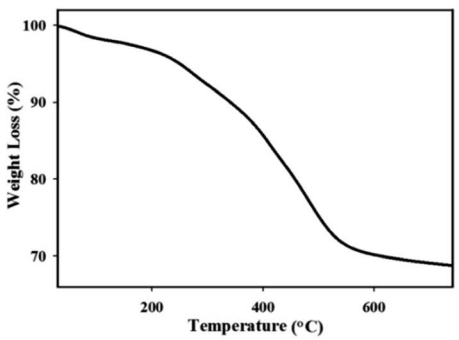

Fig. 2 TGA curve of the [(PATDBP)$(HSO_4)_2$@HNT].

the second-stage, which corresponds to the removal of organic moieties (23.41%) on the surface. These results illustrate that the IL has been covalently linked on nano-clay.

The morphology of HNTs and [(PATDBP)$(HSO_4)_2$@HNT] are shown in Fig. 3a and b. As can be seen, the tubular structure has been maintained without aggregation during the modification. The energy dispersive X-ray (EDX) results clearly display the presence of C, N, O, Al, Si, and S in the catalyst (Fig. 3c), which supports the energy-dispersive X-ray analysis (EDX) element maps results (Fig. 4). Also, these images show that the sulfur is homogeneously dispersed on the functionalized halloysite

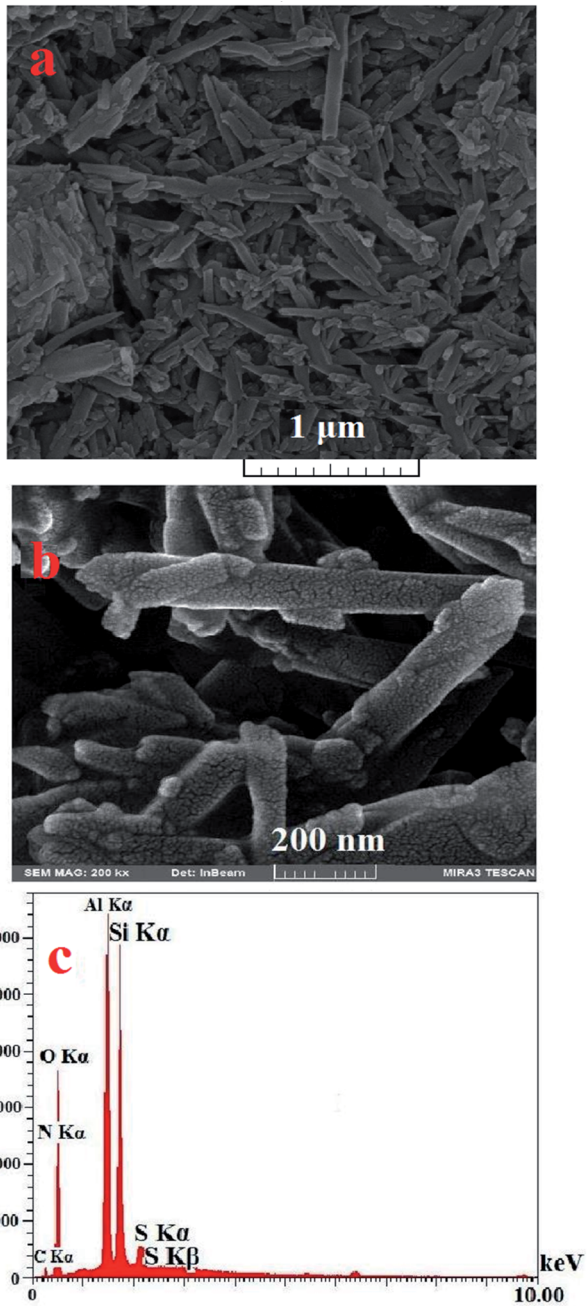

Fig. 3 (a) SEM images of HNTs (b) [(PATDBP)$(HSO_4)_2$@HNT] and (c) SEM/EDX spectrum of [(PATDBP)$(HSO_4)_2$@HNT].

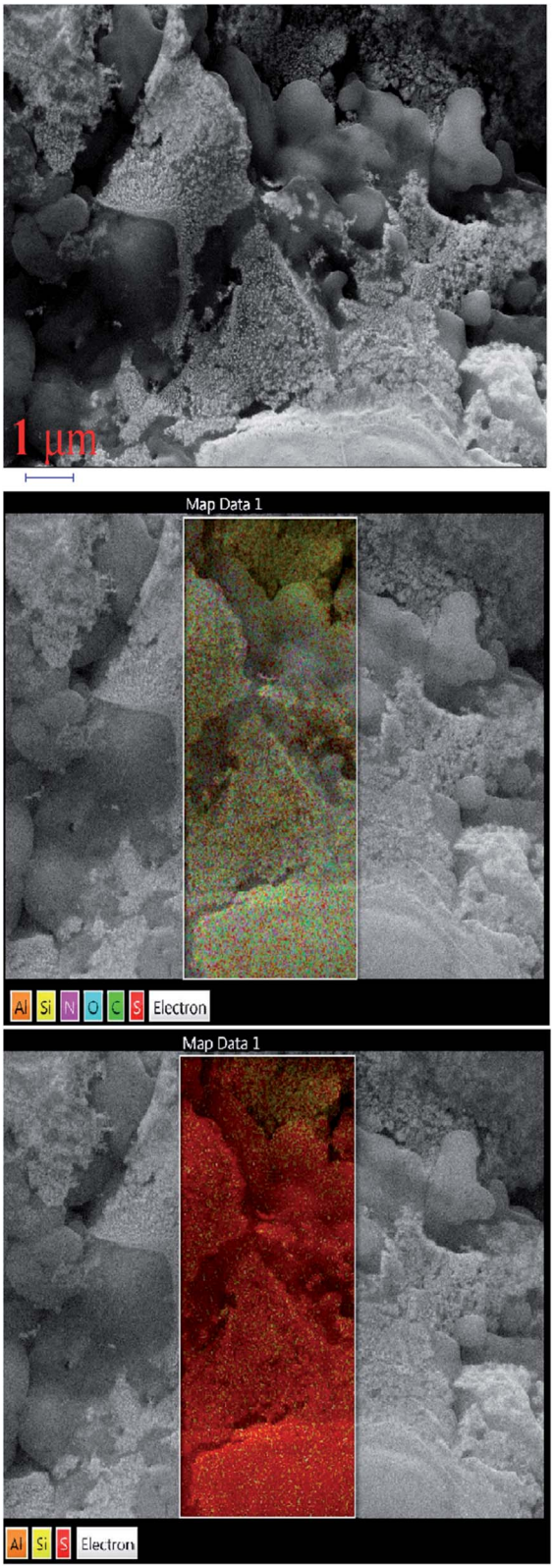

Fig. 4 Energy dispersive X-ray (EDX) mapping analysis of [(PATDBP)$(HSO_4)_2$@HNT].

nanotubes, endowing the isolation of catalytic active sites, which leads to high catalytic activity of [(PATDBP)$(HSO_4)_2$@-HNT] catalyst under mild conditions.

The nanostructure of [(PATDBP)$(HSO_4)_2$@HNT] was characterized by transmission electron microscopy (TEM). As shown in Fig. 5a and b, the catalyst possesses well-defined tubular structure. The histogram of size distribution demonstrated that the average diameter of the matrix is about 71–75 nm (Fig. 5c).

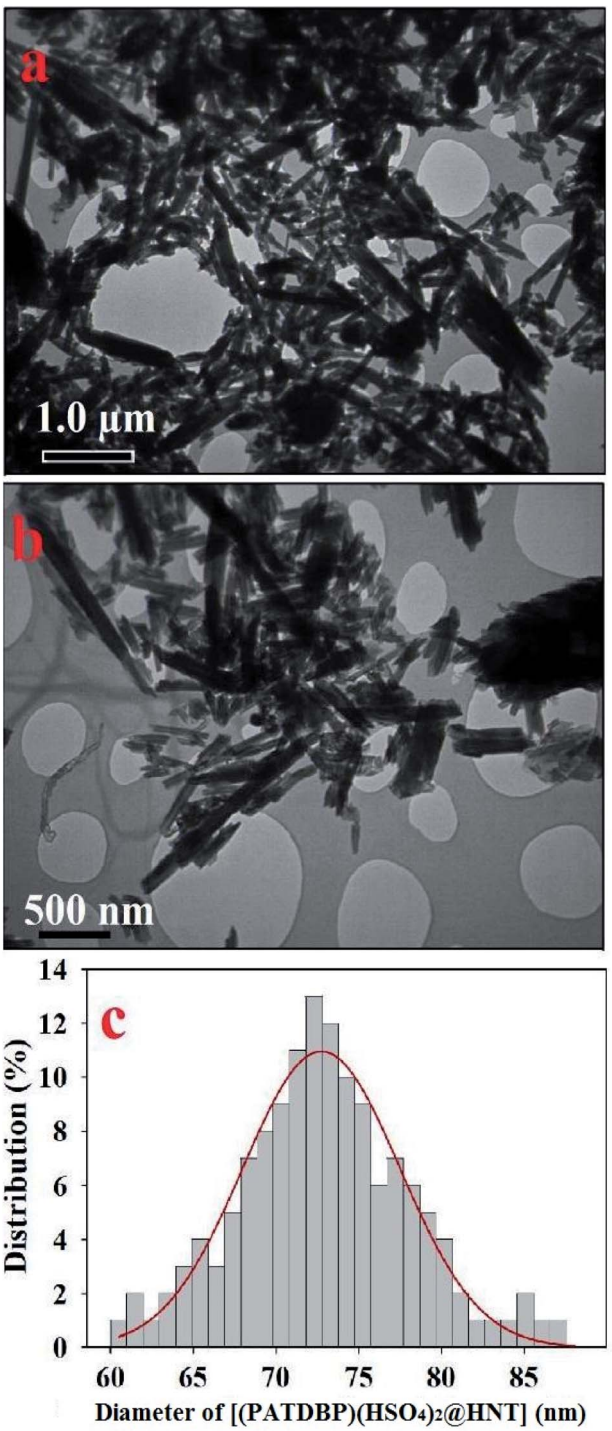

Fig. 5 TEM images in different sizes (a) 1.0 μm, and (b) 500 nm, and (c) particle size distribution for [(PATDBP)$(HSO_4)_2$@HNT].

The sulfur (HSO_4^-) content of this nanocatalyst, is 0.71 mmol g^{-1} of catalyst as obtained using elemental analysis. Also, the nitrogen content of the catalyst, presents a value of about 4.00% indicating that the amount of IL supported on the halloysite nanotubes is about 2.85 mmol g^{-1}. These results clearly show that the [(PATDBP)$(HSO_4)_2$@HNT] has been successfully synthesized.

Synthesis of naphthopyranopyrimidine derivatives catalyzed by [(PATDBP)$(HSO_4)_2$@HNT]

A model reaction of β-naphthol **1** (1 mmol), benzaldehyde **2** (1 mmol), and *N*,*N*-dimethylbarbituric acid **3** (1 mmol), was selected for the optimization of significant parameters (Table 1). When this reaction was performed in the absence of catalyst at 100 °C under solvent-free conditions, no product was observed even after 5 h (Table 1, entry 1). Next, the screening of 2 mol% of various Lewis and Brønsted acids, such as $ZnCl_2$, $AlCl_3$, $FeCl_3$, $BiCl_3$, $MnCl_2$, *p*-TSA, $NaHSO_4$, HNT and [(PATDBP)Cl_2@HNT] gave desired products in poor to moderate yields (20–60%) after 45 min under the same reaction conditions (Table 1, entries 2–10). Lastly, when [(PATDBP)$(HSO_4)_2$@HNT] catalyst was used in this three-component reaction, the desired product **4a** was obtained in 98% yield (Table 1, entry 11). This result is attributed to the high surface area of halloysite nanotube which increases the catalytic activity of this nanocatalyst. The effect of the amount of catalyst was investigated in this three-component reaction using 1–4 mol% of the nanocatalyst (entries 11–13) and 2 mol% was found to be the most suitable

Table 1 Optimization of one-pot synthesis of naphthopyranopyrimidine **4a**

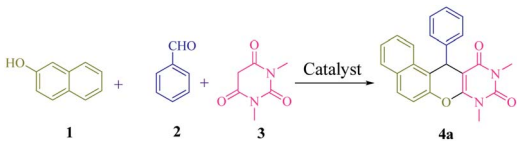

Entry	Catalyst (mol%)	*T* (°C)	Time (min)	Yield[a] (%)
1	—	100	300	0
2	$ZnCl_2$ (2)	100	45	30
3	$AlCl_3$ (2)	100	45	60
4	$FeCl_3$ (2)	100	45	30
5	$BiCl_3$ (2)	100	45	30
6	$MnCl_2$ (2)	100	45	20
7	*p*-TSA (2)	100	45	50
8	$NaHSO_4$ (2)	100	45	35
9	HNT (2)	100	45	30
10	[(PATDBP)Cl_2@HNT] (2)	100	45	45
11	[(PATDBP)$(HSO_4)_2$@HNT] (2)	100	45	98
12	[(PATDBP)$(HSO_4)_2$@HNT] (1)	100	45	70
13	[(PATDBP)$(HSO_4)_2$@HNT] (4)	100	45	98
14	[(PATDBP)$(HSO_4)_2$@HNT] (2)	25	45	10
15	[(PATDBP)$(HSO_4)_2$@HNT] (2)	70	45	50
16	[(PATDBP)$(HSO_4)_2$@HNT] (2)	120	45	98

[a] Isolated yields.

amount for this transformation (Table 1, entry 11). In addition, a survey of various temperatures (entries 14–16) revealed that the maximum yield of **4a** was obtained at 100 °C (entry 11). Utilization of the above conditions to a selection of β-naphthol, aromatic aldehydes, and *N*,*N*-dimethylbarbituric acid, enabled a diversity of naphthopyranopyrimidines **4a** in a one-pot three-component procedure in excellent yields (90–98%). The results are shown in Scheme 3 (**4a–n**). It was found that aromatic aldehydes bearing electron donating or electron withdrawing groups at either *ortho*-, *meta*- or *para*-positions of the aromatic ring, furnished the corresponding products in excellent yields and short reaction times. The structure of the products was identified by their melting points, spectral data, and elemental analysis.

Additionally, in order to further expand the applicability of this method, we carried out this three-component reaction on a gram scale. In this manner, the reaction of 10 mmol each of β-naphthol, benzaldehyde, and *N*,*N*-dimethylbarbituric acid was investigated in the presence of [(PATDBP)$(HSO_4)_2$@HNT] (0.2 mol%) at 100 °C under solvent-free conditions. Under these conditions, the desired naphthopyranopyrimidine **4a** was obtained in 70% yield after 3 h.

We also examined the selectivity of [(PATDBP)$(HSO_4)_2$@HNT] catalyst. In this respect, the competitive reaction of aromatic aldehyde (4-chlorobenzaldehyde) and aliphatic aldehyde (heptanal) with β-naphthol and *N*,*N*-dimethylbarbituric acid was studied under the same conditions. As shown Scheme 4, excellent selectivity was observed, in which 4-chlorobenzaldehyde was transformed to the related naphthopyranopyrimidine **4c** in the presence of heptanal.

Scheme 4 Selectivity between aromatic and aliphatic aldehydes.

Based on previous literatures,[9a–e] we propose a mechanistic pathway for synthesis of naphthopyranopyrimidine **4** (Scheme 5). Initially, the carbonyl group of aromatic aldehyde is activated by the catalyst to provide **I**. Subsequently, nucleophilic addition of β-naphthol to activated aromatic aldehyde provides α,β-unsaturated carbonyl compound **II**. Then, **II** is transformed to **III** in the presence of the catalyst followed by Michael addition with *N*,*N*-dimethylbarbituric acid leads to intermediate **IV**. Finally, intramolecular cyclization of **IV** in the presence of the catalyst affords intermediate **V** which upon elimination of H_2O gives the corresponding naphthopyranopyrimidine **4** and releases the catalyst for the next run.

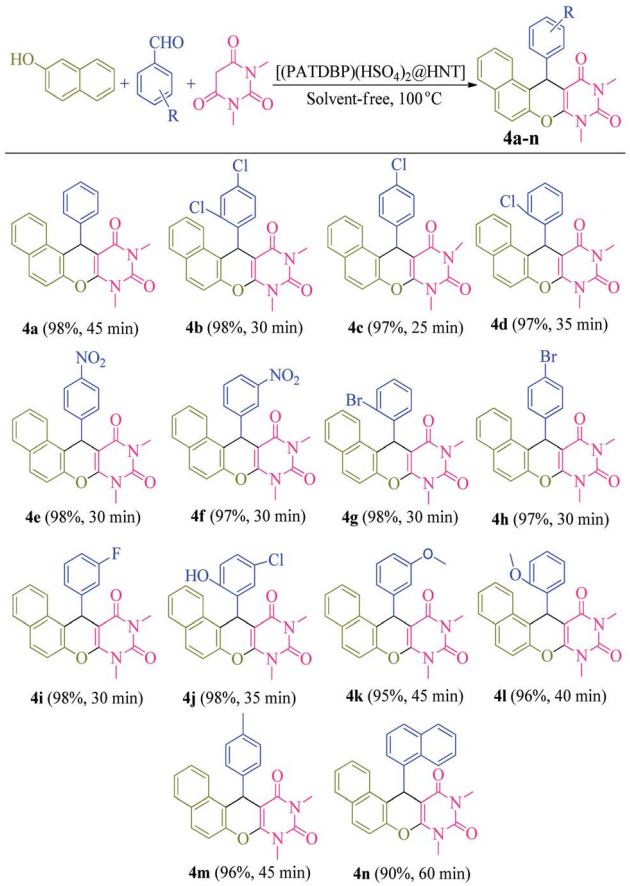

Scheme 3 Substrate scope for the synthesis of naphthopyranopyrimidines catalyzed by [(PATDBP)$(HSO_4)_2$@HNT].

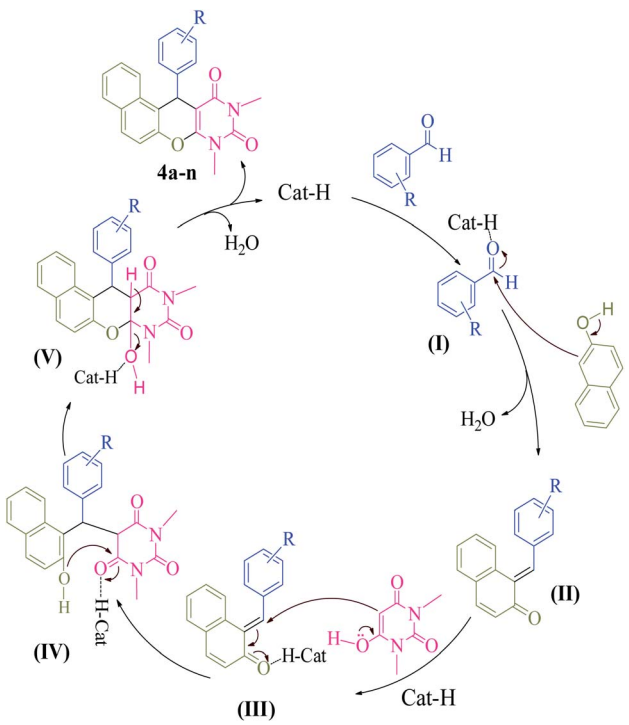

Scheme 5 A possible mechanism for synthesis of naphthopyranopyrimidines **4a–n**.

Table 2 Comparison of the results of three-component reaction of β-naphthol, 4-chlorobenzaldehyde and *N*,*N*-dimethylbarbituric acid catalyzed by [(PATDBP)$(HSO_4)_2$@HNT] with the reported results in the presence of other catalysts

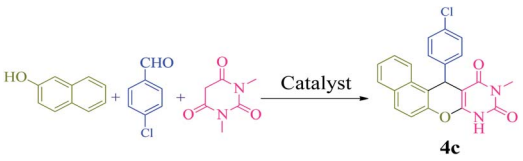

4c

Catalyst/conditions	Catalyst loading	Time (min)	Yield[a] (%)	TON[b]	TOF[c] (h^{-1})	Ref.
$KAl(SO_4)_2 \cdot 12H_2O$, PEG-400, 60 °C	15 mol%	50	84	5.6	6.7	9*a*
I_2, 120 °C, neat	10 mol%	60	75	7.5	7.5	9*b*
Nano-$ZnAl_2O_4$, MW (500 W, DMF)	0.7 mol%	10	88	125.7	785.6	9*c*
$ZrOCl_2$/nano TiO_2, solvent-free, 100 °C	3 mol%	27	83	27.6	61.3	9*d*
ZnO NPs, 110 °C	10 mol%	25	87	8.7	21.2	9*e*
$InCl_3/P_2O_5$, solvent-free, 120 °C	30/20 mol%	70/70	63/58	2.1/2.9	1.8/2.5	9*f*
Cellulose sulfamic acid/H_2O, reflux	10 mol%	240	90	9	2.25	9*g*
[(PATDBP)$(HSO_4)_2$@HNT], solvent-free, 100 °C	2 mol%	25	97	48.5	97	Present work

[a] Isolated yield. [b] TON = mol of converted substrate/mol of catalyst. [c] TOF = TON/time (h).

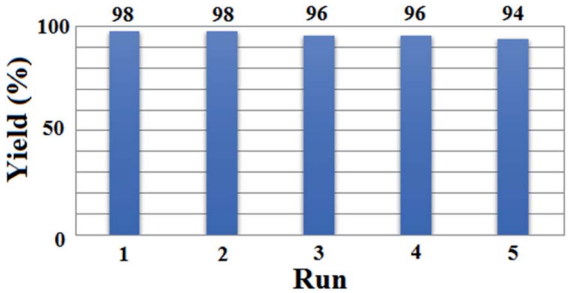

Fig. 6 Reusability of the [(PATDBP)$(HSO_4)_2$@HNT] catalyst for the synthesis of **4a**.

To indicate the efficiency of this process, we compared the result of three-component reaction of β-naphthol, 4-chlorobenzaldehyde and *N*,*N*-dimethylbarbituric acid by this method with some of those documented methods. As shown in the Table 2, the present method is superior to the previously reported methods in terms of catalyst loading, reaction time, yield, turn-over number (TON) and turn-over frequency (TOF).

The recovery and reusability of [(PATDBP)$(HSO_4)_2$@HNT] catalyst, which is remarkable from the industry and economy standpoints, was investigated in the reaction of β-naphthol (1 mmol), benzaldehyde (1 mmol), and *N*,*N*-dimethylbarbituric acid (1 mmol). At the end of the reaction, the mixture was cold to room temperature and $CHCl_3$ was added. The catalyst was easily separated from the reaction mixture by centrifugation, washed with ethanol. The recovered catalyst was dried and reused in next run. As shown the catalyst could be reused for five times without noticeable loss of its activity (Fig. 6); however, this negligible loss of the yield may be due to the slight deactivation of catalyst surface during the reaction as well as the work-up process.

Conclusions

In conclusion, we have developed [(PATDBP)$(HSO_4)_2$@HNT] as a novel and heterogeneous nanocatalyst for the efficient synthesis of naphthopyranopyrimidines *via* a one-pot three-component reaction of β-naphthol, aromatic aldehydes, and *N*,*N*-dimethylbarbituric acid under solvent-free and green conditions. Furthermore, this procedure provides noteworthy advantages, such as simple work-up process, excellent yields, high reaction rates and easy recovery of the catalyst.

Experimental section

General

The chemicals used in this work were purchased from Fluka and Merck chemical companies. HNTs were purchased from Sigma-Aldrich (Germany) chemical company. The properties of HNTs are as follows: diameter = 30–70 nm, length = 1–3 μm, cation exchange capacity = 8.0 meq g^{-1}, density = 2.53 g cm^{-3}, average hydrodynamic diameter = 399.7 nm, specific surface area ($a_{s,BET}$ = 39.156 m^2 g^{-1}), total pore volume = 0.214 cm^3 g^{-1}) and elemental compositions = $Al_2Si_2O_5(OH)_4 \cdot 2H_2O$ (1 : 1 ratio of Al/Si). Melting points were determined with a Stuart Scientific SMP2 apparatus. FT-IR spectra were recorded on a Nicolet-Impact 400D spectrophotometer. ^1H and ^{13}C NMR (400 and 100 MHz) spectra were recorded on a Bruker Avance 400 MHz spectrometer using $CDCl_3$ as solvent. Elemental analysis was performed on a LECO, CHNS-932 analyzer. Thermogravimetric analysis (TGA) was carried out on a Mettler TG50 instrument under air flow at a uniform heating rate of 20 °C min^{-1} in the range 30–740 °C. The TGA instrument was re-calibrated at frequent intervals with standards; the accuracy was always better than ±2.0%. The scanning electron microscope measurement was carried out on a Hitachi S-4700 field emission-scanning electron microscope (FE-SEM). The transmission electron

microscopy (TEM) was carried out on a Philips CM10 instrument operating at 100 kV.

General procedure for preparation of [(PATDBP)$(HSO_4)_2$@HNT]

Preparation of [PA@HNT]. First, HNT (2 g) was dispersed ultrasonically in 8 mL 3-aminopropyltriethoxysilane (APTS) for 5 min at room temperature. Then, the suspension was exposed to microwave irradiation in a closed vessel at 100 °C and a power of 25 W under constant stirring for 1 h. Finally, the precipitate (PA@HNT) was filtered, washed with ethanol (2 × 10 mL), and dried in a vacuum oven at 80 °C.

Preparation of [PAT@HNT]. The obtained PA@HNT (2 g) was dispersed in 25 mL dry THF by sonication for 10 min and then, 1,3,5-trichlorotriazine (20 mmol, 3.68 g) and DIPEA (14.4 mmol, 2.5 mL) were added and the mixture was stirred for 24 hours under N_2 at 0 °C. Finally, the precipitate PAT@HNT was filtered, washed with THF (2 × 10 mL) and acetone (10 mL), and dried in a vacuum oven at 80 °C.

Preparation of [(PATDBP)Cl_2@HNT]. A mixture of PAT@HNT (2 g) and DIPEA (11.5 mmol, 2 mL) was intensely dispersed in 17 mL pyridine and then, the reaction mixture was refluxed for 24 hours. Finally, the mixture was filtered, washed with toluene three times and dried under vacuum to afford [(PATDBP)Cl_2@HNT].

Preparation of [(PATDBP)$(HSO_4)_2$@HNT]. The nanocatalyst [(PATDBP)$(HSO_4)_2$@HNT] was generated by addition of $NaHSO_4$ (5 g) to a dispersed mixture of [(PATDBP)Cl_2@HNT] (2 g) in Mili-Q water (30 mL) at room temperature and then, was shaken for 24 hours. The resulting light brown solid was collected by filtration, washed with H_2O (3 × 10 mL) to remove the unreacted $NaHSO_4$, and finally dried in a vacuum oven at 80 °C for 5 hours.

General procedure for synthesis of naphthopyranopyrimidine derivatives catalyzed by [(PATDBP)$(HSO_4)_2$@HNT]

A mixture of β-naphthol (1 mmol), aromatic aldehyde (1 mmol), *N*,*N*-dimethylbarbituric acid (1 mmol), and [(PATDBP)$(HSO_4)_2$@HNT] (2 mol%, 28 mg) was stirred at 100 °C under solvent-free conditions for the appropriate time according to Scheme 3. The progress of the reaction was tested by TLC (eluent : petroleum ether/EtOAc, 4 : 1). After completion of the reaction, the mixture was cooled to room temperature and $CHCl_3$ (5 mL) was added. The catalyst was separated by centrifugation and washed with EtOH (5 mL). The products were obtained by recrystallization from EtOH and dried under reduced pressure. In some cases, the organic residue was purified by column chromatography on silica gel (petroleum ether/ethyl acetate) to provide the pure product in 90–98% isolated yields (Scheme 3, **4a–n**).

Abbreviations

MCR	Multicomponent reaction
HNTs	Halloysite nanotubes
ILs	Ionic liquids
APTS	(3-Aminopropyl)triethoxysilane
TCT	1,3,5-Trichlorotriazine
DIPEA	*N*,*N*-Diisopropylethylamine
p-TSA	*p*-Toluenesulfonic acid
TLC	Thin layer chromatography

Conflicts of interest

The authors declare no conflict of interest.

Acknowledgements

We are grateful to the Research Council of the University of Isfahan for financial support of this work (project number 1015).

References

1 (*a*) K. S. Egorova, E. G. Gordeev and V. P. Ananikov, *Chem. Rev.*, 2017, **117**, 7132–7189; (*b*) K. Dong, X. Liu, V. Dong, X. Zhang and S. Zhang, *Chem. Rev.*, 2017, **117**, 6636–6695; (*c*) C. Dai, J. Zhang, C. Huang and Z. Lei, *Chem. Rev.*, 2017, **117**, 6929–6983; (*d*) B. Wang, L. Qin, T. Mu, Z. Xue and G. Gao, *Chem. Rev.*, 2017, **117**, 7113–7131; (*e*) M. Watanabe, M. L. Thomas, S. Zhang, K. Ueno, T. Yasuda and K. Dokko, *Chem. Rev.*, 2017, **117**, 7190–7239; (*f*) H. J. Jiang, S. Imberti, B. A. Simmons, R. Atkin and G. G. Warr, *ChemSusChem*, 2019, **12**, 270–274.

2 (*a*) B. Sarmah and R. Srivastava, *J. Mol. Catal. A: Chem.*, 2017, **427**, 62–72; (*b*) R. S. Tukhvatshin, A. S. Kucherenko, Y. V. Nelyubina and S. G. Zlotin, *ACS Catal.*, 2017, **7**, 2981–2989; (*c*) T. Wang, W. Wang, Y. Lyu, X. Chen, C. Li, Y. Zhang, X. Song and Y. Ding, *RSC Adv.*, 2017, **7**, 2836–2841; (*d*) R. Kukawka, A. Pawlowska-Zygarowicz, J. Dzialkowska, M. Pietrowski, H. Maciejewski, K. Bica and M. Smiglak, *ACS Sustain. Chem. Eng.*, 2019, **7**, 4699–4706.

3 (*a*) M. J. Saif, H. M. Asif and M. Naveed, *J. Chil. Chem. Soc.*, 2018, **63**, 4109–4125; (*b*) X. Ding, H. Wang, W. Chen, J. Liu and Y. Zhang, *RSC Adv.*, 2014, **4**, 41993–41996; (*c*) L. Duan, W. Huang and Y. Zhang, *RSC Adv.*, 2015, **5**, 6666–6674; (*d*) Z. Hajizadeh and A. Maleki, *J. Mol. Catal.*, 2018, **460**, 87–93.

4 (*a*) N. Y. Baran, T. Baran and A. Menteş, *Appl. Clay Sci.*, 2019, **181**, 105225–105237; (*b*) N. Bálsamo, S. Mendieta, A. Heredia and M. Crivello, *J. Mol. Catal.*, 2020, **481**, 110290–110299; (*c*) V. Bertolino, G. Cavallaro, G. Lazzara, S. Milioto and F. Parisi, *Langmuir*, 2017, **33**, 3317–3323; (*d*) S. Sadjadi, M. M. Heravi, M. Malmir and B. Masoumi, *Appl. Organomet. Chem.*, 2018, **32**, 4113–4125; (*e*) S. Sadjadi, M. M. Heravi, M. Malmir and F. G. Kahangi, *Appl. Clay Sci.*, 2018, **162**, 192–203; (*f*) S. Sadjadi, M. Malmir and M. M. Heravi, *Appl. Clay Sci.*, 2019, **168**, 184–195; (*g*) S. Sadjadi, G. Lazzara, M. M. Heravi and G. Cavallaro, *Appl. Clay Sci.*, 2019, **182**, 105299–105313; (*h*) B. Eftekhari far and M. Nasr-Esfahani, *Appl. Organomet. Chem.*, 2020, **34**, 5406–5419.

5 S. M. Stagnaro, C. Volzone and L. Huck, *Procedia Mater. Sci.*, 2015, **8**, 586–591.

6 (*a*) X. Ding, H. Wang, W. Chen, J. Liua and Y. Zhang, *RSC Adv.*, 2014, **4**, 41993–41996; (*b*) L. Yu, Y. Zhang, B. Zhang and J. Liu, *Sci. Rep.*, 2014, **4**, 4551–4556; (*c*) J. Kurczewska, M. Cegłowski, B. Messyasz and G. Schroeder, *Appl. Clay Sci.*, 2018, **153**, 134–143; (*d*) Z. Long, Y. P. Wu, H. Y. Gao, Y. F. Li, R. R. He and M. Liu, *Bioconjugate Chem.*, 2018, **29**, 2606–2618; (*e*) S. Ramanayaka, B. Sarkar, A. T. Cooray, Y. S. Ok and M. Vithanage, *J. Hazard. Mater.*, 2020, **384**, 121301–121327.

7 (*a*) R. C. Cioc, E. Ruijter and R. V. Orru, *Green Chem.*, 2014, **16**, 2958–2975; (*b*) H. Liu, Y. Fang, S. Y. Wang and S. J. Ji, *Org. Lett.*, 2018, **20**, 930–933; (*c*) C. Liu, L. Zhou, D. Jiang and Y. Gu, *Asian J. Org. Chem.*, 2016, **5**, 367–372; (*d*) M. Gao, M. Zou, J. Wang, Q. Tan, B. Liu and B. Xu, *Org. Lett.*, 2019, **21**, 1593–1597; (*e*) B. Asadi, I. Mohammadpoor-Baltork, S. Tangestaninejad, M. Moghadam, V. Mirkhani and A. Landarani-Isfahani, *New J. Chem.*, 2016, **40**, 6171–6184.

8 (*a*) C. G. Neochoritis, T. Zhao and A. Dömling, *Chem. Rev.*, 2019, **119**, 1970–2042; (*b*) B. Asadi, A. Landarani-Isfahani, I. Mohammadpoor-Baltork, S. Tangestaninejad, M. Moghadam, V. Mirkhani and H. AmiriRudbari, *Tetrahedron Lett.*, 2017, **58**, 71–74; (*c*) B. Asadi, A. Landarani-Isfahani, I. Mohammadpoor-Baltork, S. Tangestaninejad, M. Moghadam, V. Mirkhani and H. Amiri Rudbari, *ACS Comb. Sci.*, 2017, **19**, 356–364; (*d*) J. Yu, F. Shi and L. Z. Gong, *Acc. Chem. Res.*, 2011, **44**, 1156–1171; (*e*) B. Asadi, I. Mohammadpoor-Baltork, V. Mirkhani, S. Tangestaninejad and M. Moghadam, *ChemistrySelect*, 2020, **5**, 7840–7848.

9 (*a*) J. M. Khurana, A. Lumb, A. Chaudhary and B. Nand, *RSC Adv.*, 2013, **3**, 1844–1854; (*b*) K. P. Kumar, S. Satyanarayana, P. L. Reddy, G. Narasimhulu, N. Ravirala and B. S. Reddy, *Tetrahedron Lett.*, 2012, **53**, 1738–1741; (*c*) M. Mohaqeq, J. Safaei-Ghomi, H. Shahbazi-Alavi and R. Teymuri, *Polycycl. Aromat. Comp.*, 2017, **37**, 52–62; (*d*) M. Mohaqeq, J. Safaei-Ghomi and H. Shahbazi-Alavi, *Acta Chim. Slovaca*, 2015, **62**, 967–972; (*e*) M. Mohaqeq and J. Safaei-Ghomi, *Monatsh. Chem.*, 2015, **146**, 1581–1586; (*f*) G. C. Nandi, S. Samai, R. Kumar and M. S. Singh, *Tetrahedron*, 2009, **65**, 7129–7134; (*g*) R. R. Chinta, V. Harikrishna, V. K. Tulam, P. S. Maincar and P. K. Dubey, *Asian J. Chem.*, 2016, **28**, 899–902.

10 A. H. Bedair, N. A. El-Hady, M. A. El-Latif, A. H. Fakery and A. M. El-Agrody, *Farmaco*, 2000, **55**, 708–714.

11 A. El-Agrody, M. Abd El-Latif, N. El-Hady, A. Fakery and A. Bedair, *Molecules*, 2001, **6**, 519–527.

12 M. Radi, S. Schenone and M. Botta, *Org. Biomol. Chem.*, 2009, **7**, 2841–2847.

13 A. H. Bedair, H. A. Emam, N. A. El-Hady, K. A. Ahmed and A. M. El-Agrody, *Farmaco*, 2001, **56**, 965–973.

14 (*a*) M. Azizi, M. Nasr-Esfahani, I. Mohammadpoor-Baltork, M. Moghadam, V. Mirkhani, S. Tangestaninejad and R. Kia, *J. Org. Chem.*, 2018, **83**, 14743–14750; (*b*) T. Ataee-Kachouei, M. Nasr-Esfahani, I. Mohammadpoor-Baltork, V. Mirkhani, M. Moghadam, S. Tangestaninejad and R. Kia, *ChemistrySelect*, 2019, **4**, 2301–2306; (*c*) T. Ataee-Kachouei, M. Nasr-Esfahani, I. Mohammadpoor-Baltork, V. Mirkhani, M. Moghadam, S. Tangestaninejad and B. Notash, *Appl. Organomet. Chem.*, 2020, **34**, 5948–5965.

15 C. Chao, J. Liu, J. Wang, Y. Zhang, B. Zhang, Y. Zhang, X. Xiang and R. Chen, *ACS Appl. Mater. Interfaces*, 2013, **5**, 10559–10564.